difference in binding affinity between **II** and **IV**, probably hinges in part on the fact that this hydroxyl group is fixed in position, so that it can be bound without substantial loss in freedom of movement with respect to the rest of the nucleoside. Other entries in Table 1, in which the effect of hydroxyl substitution is less, have considerably greater freedom of rotation. Experiments are currently under way to characterize entropic aspects of the hydration of nebularine and of its binding by adenosine deaminase. The present results imply that under favorable circumstances a single hydroxyl substituent can enhance the binding affinity of an enzyme inhibitor by a very large factor. Analogously, formation of one or two hydrogen bonds in the transition state might suffice to account for the catalytic efficiency of an enzyme of this type.

REFERENCES AND NOTES

1. R. Wolfenden, J. Kaufman, J. B. Macon, *Biochemistry* **8**, 2412 (1969); L. C. Kurz and C. Frieden, *ibid.* **22**, 382 (1983).
2. L. C. Kurz and C. Frieden, *ibid.* **26**, 8450 (1987).
3. W. Jones and R. Wolfenden, *J. Am. Chem. Soc.* **108**, 7444 (1986).
4. W. Jones, L. C. Kurz, R. Wolfenden, *Biochemistry* **28**, 1242 (1989).
5. B. Evans and R. Wolfenden, *J. Am. Chem. Soc.* **92**, 4751 (1970); *ibid.* **94**, 5902 (1972).
6. L. Frick, R. Wolfenden, E. Smal, D. C. Baker, *Biochemistry* **25**, 1616 (1986).
7. Compound **II** is approximately 8 orders of magnitude more tightly bound than the substrate or product of adenosine deamination, whereas an ideal transition-state analog for this reaction is expected to be bound at least 12 orders of magnitude more tightly than the substrate. L. Frick and R. Wolfenden, *Bioorg. Chem.* **15**, 100 (1987).
8. For the crystal structure of a compound with similar stereochemistry, see M. Shimazaki, *Chem. Pharmacol.* **31**, 3104 (1983).
9. Other estimates, not based on simple oxy-deoxy comparison of reversibly bound inhibitors, have suggested values between about −3.5 and −5.0 kcal/mol for single hydrogen bonds involving one charged and one uncharged partner [A. R. Fersht *et al.*, *Nature* **314**, 235 (1985)] and −4 kcal/mol for formation of a hydrogen bond involving a possibly charged phosphoric acid amide [P. A. Bartlett and C. K. Marlowe, *Science* **235**, 569 (1987)].
10. J. A. V. Butler, *Trans. Faraday Soc.* **33**, 229 (1937).
11. M. Meot-Ner and L. W. Sieck, *J. Am. Chem. Soc.* **108**, 7525 (1986).
12. S. J. Weiner *et al.*, *ibid.* **106**, 765 (1984).
13. Steric hindrance appears less likely to interfere with the binding of **IV** than of **II**, but it seems possible that a water molecule might be "trapped" in the complex of the enzyme with **IV** (but not with **II**). Because formation of such a complex would not occur unless it were energetically favorable as compared with the binding of **IV** alone, the presence of such a trapped water molecule would not in itself tend to destabilize the complex. These considerations suggest that enzyme distortion or trapping of a water molecule, if these occur, should tend to level the observed difference in binding affinities between **II** and **IV** rather than help to explain why this difference is so large.
14. D. K. Wilson, F. B. Rudolph, M. L. Harrison, R. E. Kellems, F. A. Quiocho, *J. Mol. Biol.* **200**, 613 (1988).
15. W. P. Jencks, *Proc. Natl. Acad. Sci. U.S.A.* **78**, 4046 (1981).
16. I. P. Street, C. R. Armstrong, S. G. Withers, *Biochemistry* **25**, 6021 (1986).
17. M. P. Dale, H. E. Ensley, K. Kern, K. A. R. Sastry, L. D. Byers, *ibid.* **24**, 3530 (1985).
18. S. G. Cohen *et al.*, *Bioorg. Chem.* **15**, 237 (1987).
19. D. H. Rich, B. J. Moon, S. Harbeson, *J. Med. Chem.* **27**, 417 (1984).
20. D. H. Rich, *ibid.* **28**, 263 (1984).

21. Supported by grant GM-18325 from the National Institutes of Health.

25 October 1988; accepted 20 December 1988

Direct Measurements of Sliding Between Outer Doublet Microtubules in Swimming Sperm Flagella

CHARLES J. BROKAW

The relative motion of 40-nanometer gold beads bound to the exposed outer doublet microtubules of demembranated sea urchin sperm flagella has been observed and photographed during adenosine triphosphate (ATP)–reactivated swimming. This direct demonstration and measure of sliding displacements between outer doublet microtubules in actively bending flagella verifies the original sliding microtubule model for ciliary bending that was established by electron microscopy of fixed cilia and provides a new, functional measure for the diameter of the flagellar axoneme of 132 ± 8 nanometers.

SLIDING BETWEEN OUTER DOUBLET microtubules has been assumed to occur during, and to be responsible for, the bending of cilia and flagella. The occurrence of sliding during bending was inferred from electron micrographs of fixed cilia (*1*), from observations of sliding during flagellar disintegration (*2*), and from the characteristics of certain unusual bending patterns (*3*). Direct visualization and measurement of sliding in actively bending flagella of ATP-reactivated, demembranated, sea urchin spermatozoa has now been achieved by using gold beads as markers of positions on the outer doublet microtubules.

Preparations of demembranated spermatozoa were incubated in suspensions containing gold beads and then diluted into solutions containing MgATP for observation of motility (*4–8*). Beads [or bead aggregates, which cannot be easily distinguished from individual beads by light microscopy (*9, 10*)] attached to the flagellar axoneme and remained in position for hundreds of beat cycles; they were not dragged or propelled to either end of the flagellum. Demembranated sperm flagella decorated with beads swam with nearly normal bending patterns, similar to those of undecorated flagella in the same preparation (Fig. 1A).

Under ideal circumstances, where a pair of beads is separated by a distance of 1 μm or less along the axoneme, direct inspection of a sequence of photographs (for example, Fig. 1B) revealed that the two beads moved closer together and then farther apart as the flagellum bent. When low MgATP concentrations were used to obtain flagellar beat frequencies of 1 Hz or less, these movements were also seen by direct visual observation, with the use of dark-field light microscopy. The relative movements of three beads indicating three independently sliding doublet microtubules can be seen in Fig. 1D, in which portions of a photograph were cut and realigned for direct comparison of the positions of bead images at the extremes of the beat cycle.

Computer-assisted measurements of the distances between beads were carried out on digitized portions of the photographic negatives (*11*). Usually, measurements were made only when a pair of beads, separated by 1 to 4 μm, was located in a straight region between bends on the flagellum (Fig. 2A). The angle between these straight regions and the axis of the sperm head was the measure of shear angle. Amplitudes of oscillation of bead separation ranging from 0 to 0.4 μm were measured. Occasionally, measurements on closely spaced beads were made throughout the bend cycle (Fig. 2C); in these cases the small error caused by measuring straight-line distance between the beads rather than distance along the curve of the flagellum was ignored.

Relative movement of beads attached to outer doublet microtubules could be caused either by interdoublet sliding or by contraction and elongation of outer doublets (Fig. 3). Two properties of the movements clearly discriminate between these two possibilities. First, bead movements resulting from interdoublet sliding have peak amplitudes in phase with either positive or negative shear angle, as shown by the sliding model in Fig. 3 and the data in Fig. 2. Bead movements resulting from length changes have peak

Division of Biology, California Institute of Technology, Pasadena, CA 91125.

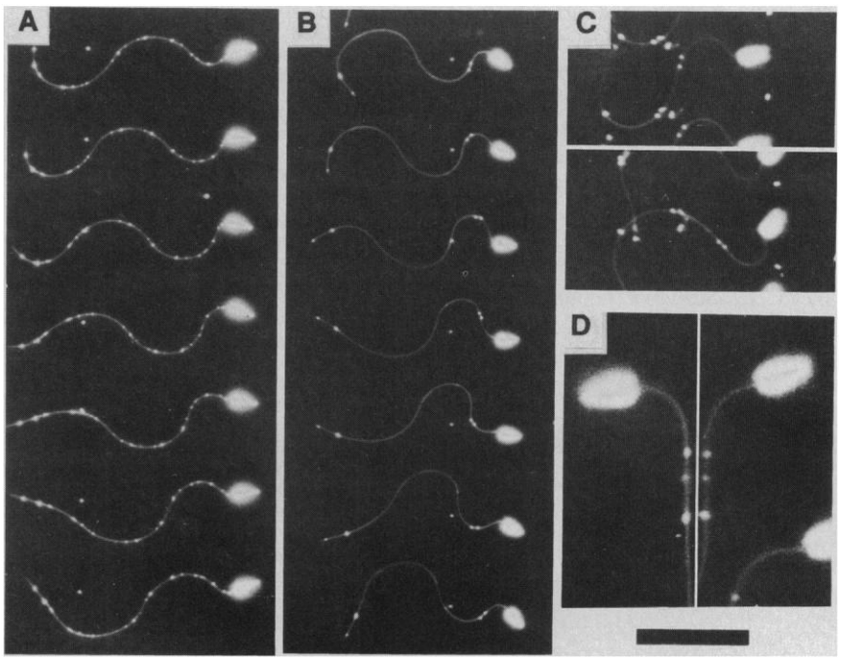

Fig. 1. Portions of multiple exposure, dark-field photomicrographs taken on moving film, showing ATP-reactivated movement of demembranated spermatozoa from the sea urchin, *Lytechinus pictus* (*4*). (**A** and **B**) Spermatozoa reactivated with 80 μM MgATP and 2 mM lithium acetate; flash rate, 120 Hz. (**C**) Spermatozoon reactivated with 6 μM MgATP and 4 mM lithium acetate; 0.40 s between these two images. (**D**) Images selected to show the extremes of the bending cycle, separated by a half cycle (0.45 s), for a flagellum carrying three beads attached to different doublet microtubules; reactivated as in (C). In (D), the measured separations of the upper bead pair were 2.25 μm at a shear angle of −1.75 rad and 2.13 μm at a shear angle of 1.25 rad, corresponding to sliding of −40 nm/rad. The measured separations of the lower bead pair were 3.50 μm at −1.78 rad and 3.23 μm at 1.24 rad, corresponding to sliding of −90 nm/rad. Sliding between the top and bottom bead was therefore −130 nm/rad. (A) and (B) were taken with a 100× objective; (C) and (D) with a 40× objective. Scale bar indicates 20 μm in (A), (B), and (C); 10 μm in (D).

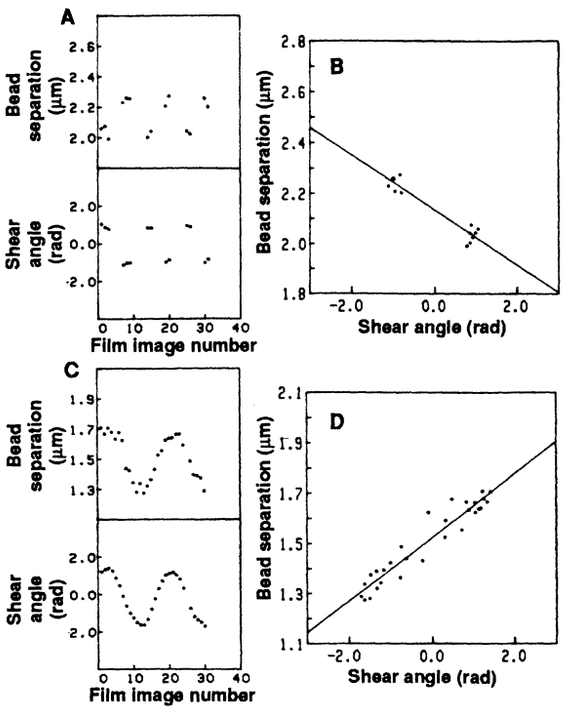

Fig. 2. Examples of measurements of bead separation and shear angle (*11*). (**A** and **C**) Measurements plotted as functions of time (film image number at 20 images per second). (**B** and **D**) Measurements replotted as bead separation versus shear angle. (C) and (D) are measurements on the bead pair closest to the sperm head in Fig. 1C.

amplitudes in phase with the curvature of the flagellum, 90° out of phase with the shear angle (Fig. 3, contraction model). Second, bead movements resulting from length changes accumulate through a bend, giving maximal effects with measurements between two beads at each end of a bend (Fig. 3, contraction model, filled circles). As the distance between a pair of beads diminishes, the bead displacements also become small (Fig. 3, contraction model, open circles). The large movements observed with bead pairs only 1 μm apart can only be accounted for by sliding between microtubules.

These observations therefore provide direct confirmation of the "central dogma" of ciliary motility: that bending of the axoneme during the beat cycle is associated with sliding between outer doublet microtubules rather than with contraction and elongation of the doublets. This dogma was originally established from electron micrographs of cilia fixed in bent positions (*1, 12*), with the assumption that the conformation of the outer doublet microtubules is faithfully preserved during fixation for electron microscopy. Important additional support was obtained from direct observations of ATP-dependent sliding disintegration of flagellar axonemes, after protease digestion to disrupt the structures that are presumed to limit sliding in intact axonemes and to convert sliding into bending of the flagellum (*2*).

The measurements of bead movements also provide a direct, quantitative measure of microtubule sliding during active flagellar bending. Unfortunately, the usefulness of this measure for analyzing the generation of bending by sliding is limited because the doublets on which particular beads are riding are not readily identifiable. In the absence of this information, the distribution of the movements of a large sample of beads, assumed to attach randomly to outer doublet microtubules, was examined. Data are presented for 51 demembranated spermatozoa, 19 of which carried more than one measured pair of beads, that were reactivated with low MgATP concentrations (to obtain beat frequencies of 1 to 2 Hz and bend angles of 2 to 3.5 rad) and photographed at 20 images per second. Because there is little angular oscillation of the sperm head at these low beat frequencies, measurements of flagellar angle referred to the axis of the sperm head are likely to be directly proportional to sliding within the flagellum (see below). For each measured bead pair, the slope of the linear regression line for bead separation versus shear angle was determined (Fig. 2, B and D). This slope measures the bead movements in phase with shear angle that result from interdoublet sliding. When angular measurements are an

accurate measure of shear within the flagellum, the slope, with units of nanometers per radian, is equal to the distance in nanometers, measured parallel to the plane of bending, between two outer doublet microtubules on which the beads are riding. This distance is referred to as "doublet separation" (Fig. 4, inset). The distribution of the absolute values of measured doublet separation for a random sample of 81 pairs of beads is shown in Fig. 4. Each measurement is shown as a horizontal line representing the 90% confidence interval; the measurements have been arranged in order of increasing magnitude from top to bottom of the graph.

The solid points in Fig. 4 show the expected distribution of sliding between any two doublets (not necessarily adjacent) as doublet separations, parallel to the bending plane, calculated from the geometry of the axonemal cross section on the assumption of independent sliding without changes in the doublet length (Fig. 4, inset). The calculated values of doublet separation for the 81 possible combinations of two doublets that can result from random attachment of two beads have been arranged in order of increasing magnitude from top to bottom of the graph (*13*).

Similarity between the shapes of the experimental and theoretical distributions in Fig. 4 indicates conformity with the original sliding microtubule model based on independent sliding of each doublet (*1*). In particular, the results in Fig. 4 do not show the bimodal distribution, with one large group of near-zero doublet separations and another large group of near-maximal doublet separations, that would be expected if one group of doublets, such as 8, 9, 1, 2, and 3, slides as a unit, without internal sliding, relative to another subgroup (4, 5, 6, and 7), during the normal bending cycle. This idea is suggested by several recent studies of disintegrating axonemes (*14, 15*) in which groups such as these were seen to remain associated after sliding disintegration. The doublet association seen in disintegrating axonemes can be explained by the occurrence of splitting in regions of maximal sliding displacements, without the requirement that sliding be restricted to these intergroup boundaries (*14*). Examples such as Fig. 1D, where the bead movements indicate independent sliding of three different doublets, also provide direct evidence against the idea that sliding during bending can only occur between the two groups that remain associated after disintegration.

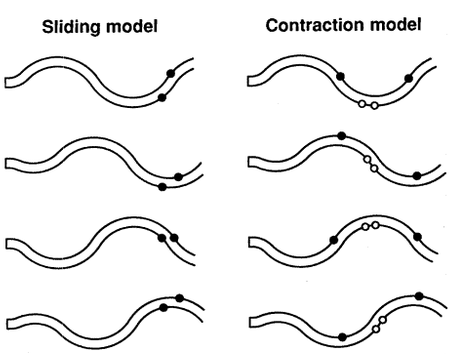

Fig. 3. Diagrams illustrating bead movements predicted by two models for the generation of flagellar bending. The flagellum is represented by two lines corresponding to outer doublet microtubules attached together at the base of the flagellum. To produce a compact figure, the doublet separation and bead sizes are greatly exaggerated relative to the lengths of the bends propagating along the flagellum. For the sliding model, the distances from the base of the flagellum to the points of bead attachment, measured along the doublet to which each bead is attached, remain constant as the flagellum bends. For the contraction model, the bead positions projected onto a center line between the doublets remain constant as the flagellum bends.

Similarity between the positions of the experimental and theoretical distributions in Fig. 4 depends on the value of axonemal diameter used for the theoretical calculations. The value of 132 ± 8 nm, obtained from weighted least-squares fitting of the data points to the model distribution (*16*), represents a functional measure of axonemal diameter. It is the diameter of the circle passing through the neutral surface of each doublet, that is, the surface that undergoes no longitudinal compression or extension when the doublet bends. If this surface is approximately at the center of the cross section of the doublet, then the diameter of the circle corresponding to the outer edges of the doublets is 158 nm.

The value of 158 nm for the diameter is less than the commonly used value of 200 nm obtained from electron microscope images. However, values obtained by electron microscopy vary according to the conditions of sample preparation. Values of 190 to 200 nm were obtained with flagella or cilia prepared for electron microscopy with buffers that promote detachment of dynein crossbridges between outer doublet microtubules, but values of 151 to 165 nm were reported with buffers that promote crossbridge attachment (*17*). Therefore, for calculating sliding displacements between axonemal doublets in actively bending flagella, the functional diameter of 132 nm should be used. This value corresponds to a center-to-center spacing between adjacent doublets of 45 nm. For four doublets on one side of the bending plane, the average interdoublet spacing, projected onto the bending plane, is 32 nm and is the value that should be used to convert angular measurements to average sliding between doublets.

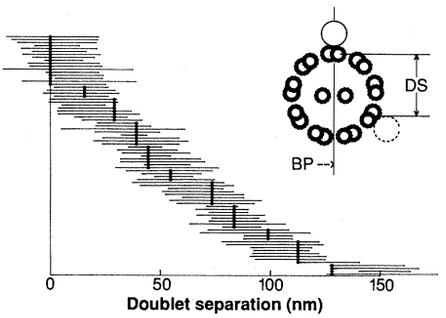

Fig. 4. Absolute values of doublet separation, arranged in order of increasing magnitude from top to bottom of the graph. Values obtained from bead measurements are shown by horizontal lines representing the 90% confidence interval for the slopes determined as in Fig. 2, B and D, using Student's t distribution and the variance for the slope calculated from the linear regression. Values calculated from axonemal geometry (*13*) for an axonemal diameter of 132 nm (tubule centers) or 158 nm (overall) are shown by solid points. The inset shows microtubule locations in an axonemal cross section and identifies the doublet separation (DS) for a pair of beads (shown by the large open circles) and the bending plane (BP).

The above discussion has emphasized the agreement between direct measurements of sliding obtained from bead movements and indirect calculations based on angular measurements of flagellar bending. The considerably greater effort required for the direct measurements is justified under conditions where the angular measurements are unreliable. Calculation of the shear angle from the observed bending requires measurement of the orientation of the basal end of the flagellum, where sliding is assumed to be 0 (*1, 12*). With swimming sperm flagella, the orientation of the axis of the sperm head is normally used to indicate the orientation of the basal end of the flagellum. This assumption can introduce significant errors if there are changes in the angle between the head axis and the base of the flagellum as the head of a swimming sperm swings from side to side. Such changes may be responsible for observations of apparently nonuniform patterns of microtubule sliding (oscillatory synchronous sliding) during the bending cycle in swimming spermatozoa—patterns that are difficult to simulate with simple models for flagellar bend propagation (*18*). Bead measurements of sliding provide an independent measure of microtubule sliding that can resolve this uncertainty and provide an accurate description of sliding patterns in swimming sperm flagella (*19*).

Measurement of sliding by measurement of bead movement can also be used when sliding is not causing bending. The underlying mechanism for flagellar oscillation might be a low-amplitude shear oscillation that is amplified when flagella bend (*20*). With the

use of beads as markers, this low-amplitude shear oscillation should be measurable in the absence of bending in fragments of demembranated flagella examined under conditions appropriate for reactivating the bending of intact flagella.

These applications will be facilitated by development of more automatic and higher precision methods for photographic image analysis to obtain measurements of bead separation in both straight and curved regions of a flagellum. Other recent work has demonstrated the ability of digital image-processing methods to extract positional information from light microscopic images at nanometer dimensions, well below the resolving distance of light microscopy (*10, 21*).

REFERENCES AND NOTES

1. P. Satir, *J. Cell Biol.* **39**, 77 (1968).
2. K. E. Summers and I. R. Gibbons, *Proc. Natl. Acad. Sci. U.S.A.* **68**, 3092 (1971).
3. C. J. Brokaw, *J. Exp. Biol.* **43**, 155 (1965); C. Shingyoji, A. Murakami, K. Takahashi, *Nature* **256**, 269 (1978).
4. Spermatozoa were demembranated with Triton X-100, activated by incubation for 90 s with cyclic adenosine monophosphate and ATP, and treated for 30 s with 2 m*M* Ca^{2+} to extract calmodulin (*5*). A 100-μl aliquot was then added to 1 ml of reactivation solution lacking polyethylene glycol or methyl cellulose, containing 100 μl of a suspension of 40-nm gold beads (Janssen Life Science Products, Piscataway, NJ). After 2 min, a 100-μl portion of this mixture was diluted with 1 ml of reactivation solution containing, in addition to standard components (*5*), 1 to 10 m*M* lithium acetate to increase bend angles (*6*) and 0.1 to 0.2% methyl cellulose to decrease the bending wavelengths (7). Spermatozoa swimming next to a water-oil interface were observed in thin hanging-drop preparations with the use of a well slide filled with mineral oil (*8*). All procedures and observations were carried out at 18°C.
5. C. J. Brokaw, in *Echinoderm Gametes and Embryos*, T. E. Schroeder, Ed. (*Methods in Cell Biology*, vol. 27) (Academic Press, New York, 1987), pp. 41–56.
6. ———, *J. Cell Biol.* **105**, 1789 (1987); in *Cell Movement I, The Dynein ATPases*, F. D. Warner, P. L. Satir, I. R. Gibbons, Eds. (Liss, New York, 1989), pp. 267–279.
7. ———, *J. Exp. Biol.* **62**, 701 (1975).
8. ——— and B. Benedict, *Arch. Biochem. Biophys.* **125**, 770 (1968).
9. M. de Brabender, R. Nuydens, G. Geuns, M. Moeremans, J. De May, *Cell Motility Cytoskeleton* **6**, 105 (1986).
10. B. J. Schnapp, J. Gelles, M. P. Sheetz, *ibid.* **10**, 47 (1988).
11. Selected portions of the photographic negatives were digitized at 2048 by 768 pixels (21.5 pixel/μm), 256 gray levels, with an Eikonix 850 camera (Eikonix Corporation, Bedford, MA) and transferred to a Hewlett-Packard 320 microcomputer. A portion of the image was displayed, and a line parallel to the head axis was entered manually. A second line was entered, parallel to the flagellum and transecting the images of two beads selected for measurement. The angle between these two lines was used as a measure of shear angle at the location of the beads. Pixel intensity along the line through the beads was calculated for a band of pixels, usually 11 pixels in width, centered on the line, and displayed. By visual inspection, a threshold was selected to retain only the peaks corresponding to the two beads. The position of the centroid of each peak was then computed from intensity values above the threshold and used to obtain the distance between the two beads. This is a simplified, one-dimensional version of the procedure described by Gelles *et al.* (*21*).
12. F. D. Warner and P. Satir, *J. Cell Biol.* **63**, 35 (1974).
13. The values are the 81 values of 61 nm times the absolute value of the function $\cos[0.698\ (n-1)] - \cos[0.698\ (m-1)]$ evaluated for all values of n,m, from 1 to 9. In this calculation it is assumed that the axonemal cross section is circular (or elliptical but symmetric around the bending plane), that the bending plane passes through doublet 1 and the 5-6 bridge, and that the axonemal diameter, measured at the center of the doublets, is 132 nm in the bending plane. This distribution is appropriate either for the case where each bead attaches to just one doublet or for the case where each bead attaches to two adjacent doublets. If both types of attachment occur, then there are 4×81 possible combinations, and the distribution of "doublet separation" is smoother.
14. W. S. Sale, *J. Cell Biol.* **102**, 2042 (1986).
15. S. L. Tamm and S. Tamm, *ibid.* **99**, 1364 (1984).
16. The reciprocal of the square of the 90% confidence interval was used as a weighting factor. The root-mean-square error of 8.4 nm remaining after least squares fitting is in this case an estimate of the standard error for the diameter, because $n - 1 = 80$ degrees of freedom were removed by the process of ordering the distribution of measured values.
17. I. R. Gibbons, in *Molecules and Cell Movement*, S. Inoué and R. E. Stephens, Eds. (Raven, New York, 1975), pp. 207–231; F. D. Warner, *J. Cell Biol.* **78**, R19 (1978).
18. I. R. Gibbons, *Symp. Soc. Exp. Biol.* **35**, 225 (1982); C. J. Brokaw, *Biophys. J.* **48**, 633 (1985).
19. The data from the sample presented here do not address this question, because movement at low ATP concentrations was chosen to avoid the oscillations in head orientation associated with nonuniform sliding patterns (7).
20. C. J. Brokaw and T. F. Simonick, in *Cell Motility*, R. Goldman, T. Pollard, J. Rosenbaum, Eds. (Cold Spring Harbor Laboratory, Cold Spring Harbor, NY, 1976), pp. 933–940; *J. Cell Sci.* **23**, 227 (1977); C. J. Brokaw, *Proc. Natl. Acad. Sci. U.S.A.* **72**, 3102 (1975).
21. J. Gelles, B. J. Schnapp, M. Sheetz, *Nature* **331**, 450 (1988).

22. I thank S. M. Nagayama for laboratory assistance and M. Sheetz for the suggestion that uncoated gold beads should adhere to axonemal microtubules. Supported by NIH grants GM-18711 and RR-07003.

12 October 1988; accepted 12 January 1989

Histamine Is an Intracellular Messenger Mediating Platelet Aggregation

SATYA P. SAXENA, LORNE J. BRANDES, ALLAN B. BECKER, KEITH J. SIMONS, FRANK S. LABELLA, JON M. GERRARD*

Inhibition of human platelet aggregation by *N,N*-diethyl-2-[4-(phenylmethyl)phenoxy]ethanamine-HCl (DPPE), a novel antagonist of histamine binding, suggested that histamine might serve a critical role in cell function. Phorbol-12-myristate-13-acetate (PMA) or collagen was found to increase platelet histamine content in parallel with promotion of aggregation. Inhibitors of histidine decarboxylase (HDC) suppressed both aggregation and the elevation of histamine content, whereas DPPE inhibited aggregation only. In saponin-permeabilized platelets, added histamine reversed the inhibition by DPPE or HDC inhibitors on aggregation induced by PMA or collagen. The results indicate a role for histamine as an intracellular messenger, which in platelets promotes aggregation.

HISTAMINE IS A WELL-ESTABLISHED extracellular messenger in numerous physiological and pathophysiological conditions, including allergies, inflammation, gastric acid secretion, neurotransmission, cardiac dysfunction, and uterine contraction, and is implicated in others such as immunoregulation (*1*). Almost 30 years ago, Kahlson *et al.* (*2*) suggested that newly formed histamine might be an important mediator of cell growth. Histidine decarboxylase (HDC) activity, the ability of cells and tissues to form histamine, has been correlated with cell multiplication and growth (*3*). Studies of DPPE, an antiproliferative agent that antagonizes histamine binding at a novel (non-H_1, non-H_2, non-H_3) affinity site that binds histamine in micromolar amounts (*4*), showed that DPPE inhibits platelet aggregation stimulated by PMA, a tumor promoter usually considered to act primarily through activation of protein kinase C (*5*). However, DPPE did not inhibit protein kinase C–induced phosphorylation of a platelet M_r 47,000 protein (p47) (*6*). Thus, the antiaggregatory effect of DPPE is not due to antagonism of protein kinase C. Since PMA in-

S. P. Saxena and J. M. Gerrard, Manitoba Institute of Cell Biology and Department of Pediatrics, University of Manitoba, Winnipeg, Manitoba, Canada R3E 0V9.
L. J. Brandes, Manitoba Institute of Cell Biology and Departments of Medicine and Pharmacology and Therapeutics, University of Manitoba, Winnipeg, Manitoba, Canada R3E 0V9.
A. B. Becker, Department of Pediatrics, University of Manitoba, Winnipeg, Manitoba, Canada R3E 0V9.
K. J. Simons, Faculty of Pharmacy, University of Manitoba, Winnipeg, Manitoba, Canada R3T 2N2.
F. S. LaBella, Department of Pharmacology and Therapeutics, University of Manitoba, Winnipeg, Manitoba, Canada R3E 0V9.

*To whom correspondence should be addressed.